01 Apr 2014

Bi-Harmonic Cantilever Design for Improved Measurement Sensitivity in Tapping-Mode Atomic Force Microscopy

M. Loganathan

Douglas A. Bristow
Missouri University of Science and Technology, dbristow@mst.edu

Recommended Citation

M. Loganathan and D. A. Bristow, "Bi-Harmonic Cantilever Design for Improved Measurement Sensitivity in Tapping-Mode Atomic Force Microscopy," *Review of Scientific Instruments*, vol. 85, no. 4, American Institute of Physics (AIP), Apr 2014.
The definitive version is available at https://doi.org/10.1063/1.4870409

Bi-harmonic cantilever design for improved measurement sensitivity in tapping-mode atomic force microscopy

Muthukumaran Loganathan, and Douglas A. Bristow

Citation: Review of Scientific Instruments **85**, 043703 (2014); doi: 10.1063/1.4870409
View online: https://doi.org/10.1063/1.4870409
View Table of Contents: http://aip.scitation.org/toc/rsi/85/4
Published by the American Institute of Physics

Bi-harmonic cantilever design for improved measurement sensitivity in tapping-mode atomic force microscopy

Muthukumaran Loganathan and Douglas A. Bristow[a)]
Department of Mechanical and Aerospace Engineering, Missouri University of Science and Technology, Rolla, Missouri 65401, USA

(Received 21 February 2014; accepted 20 March 2014; published online 10 April 2014)

This paper presents a method and cantilever design for improving the mechanical measurement sensitivity in the atomic force microscopy (AFM) tapping mode. The method uses two harmonics in the drive signal to generate a bi-harmonic tapping trajectory. Mathematical analysis demonstrates that the wide-valley bi-harmonic tapping trajectory is as much as 70% more sensitive to changes in the sample topography than the standard single-harmonic trajectory typically used. Although standard AFM cantilevers can be driven in the bi-harmonic tapping trajectory, they require large forcing at the second harmonic. A design is presented for a bi-harmonic cantilever that has a second resonant mode at twice its first resonant mode, thereby capable of generating bi-harmonic trajectories with small forcing signals. Bi-harmonic cantilevers are fabricated by milling a small cantilever on the interior of a standard cantilever probe using a focused ion beam. Bi-harmonic drive signals are derived for standard cantilevers and bi-harmonic cantilevers. Experimental results demonstrate better than 30% improvement in measurement sensitivity using the bi-harmonic cantilever. Images obtained through bi-harmonic tapping exhibit improved sharpness and surface tracking, especially at high scan speeds and low force fields. © *2014 AIP Publishing LLC*. [http://dx.doi.org/10.1063/1.4870409]

I. INTRODUCTION

Conventional tapping-mode atomic force microscopy (AFM)[1] involves exciting the micro cantilever probe near its resonant frequency so that the sharp tip at the end of the cantilever taps intermittently on the surface of interest. Changes in the sample height cause a change in the tapping amplitude and/or phase. A feedback control loop monitoring the amplitude raises (or lowers) the sample in order to maintain constant amplitude and phase. The distance that the sample is raised (or lowered) corresponds to the change in sample height and is used to generate the sample image.

The quality of the AFM image is a combination of a number of factors that affect the signal-to-noise ratio (SNR). When precise measurements are needed, or in challenging scenarios such as high-speed AFM[2,3] and non-contact tapping AFM,[4–6] high SNR is critically important. Efforts to improve SNR have focused on the optical lever[7,8] and the electronics, particularly the sampling rate and algorithms used in the feedback loop.[9,10] Thermal noise in the cantilever can be reduced by using smaller cantilevers and in some cases a larger optical spot size.[11]

The harmonic motion of the cantilever has also been the focus of a great deal of study. Though the steady state tapping trajectory is predominantly sinusoidal with the same fundamental frequency as the driving signal, it also contains higher harmonic components [12–14] due to the nonlinear tip-sample interaction. The higher harmonics can be correlated to surface inhomogeneities[15–17] and electrostatic forces.[18,19] Alternatively, significant compositional sensitivity can be achieved by driving the cantilever with multi-frequency signals. Garcia *et al.* proposed a method to obtain compositional maps by exciting the first two modes of the cantilever [20–22] and monitoring the phase of the second eigenmode. Another proposed approach[23] is to design new cantilevers whose eigenmodes coincide with the higher harmonics. These designs amplify the signal-to-noise ratio in order to measure sample viscoelasticity and adhesion.

Although cantilever harmonic motion has been well studied, it has only recently been considered for its effect on measurement sensitivity. In previous work by the authors,[24] it was observed that certain multi-frequency drive signals could improve the measurement sensitivity. Certain shapes, such as the broad valley, bi-harmonic trajectory demonstrated a 20% improvement in measurement sensitivity in experiments. In this article, we build on these results by presenting a theory for AFM trajectory shaping and a new cantilever profile that is designed to amplify the trajectory shaping effect. In Sec. II we present the theoretical development of tip trajectory shaping. Section III discusses mathematical modeling, design, and fabrication of bi-harmonic cantilevers. Experimental results exhibiting improved measurement sensitivity, and sharper surface images obtained for several imaging scenarios are presented in Sec. IV. This is followed by conclusions in Sec. V.

II. TRAJECTORY SHAPING

AFM probes in tapping mode are known to have a dominantly sinusoidal response across the entire approach-retract range.[25] However, it is possible to introduce additional harmonics into the trajectory of the probe by injecting additional harmonics (with very large amplitude) into the tapping piezo drive signal. We refer to this process as trajectory shaping and find that shaped trajectories undergo significant shape change

a)Author to whom any correspondence should be addressed. Electronic mail: dbristow@mst.edu

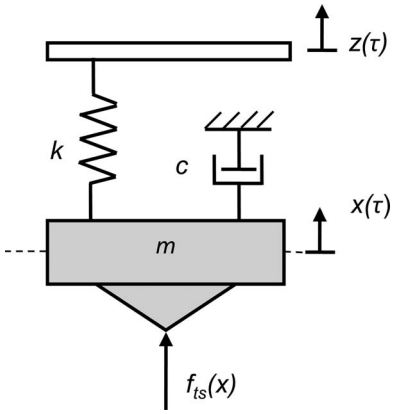

FIG. 1. Simple cantilever model driven by base excitation.

across the approach-retract range. The theory behind trajectory shaping is shown first and then used to shape trajectories that can be used for significantly improving measurement sensitivity.

A. Trajectory shaping theory

Consider the single-mode model of a base-excited cantilever probe shown in Figure 1,

$$m\ddot{x}(t) + c\dot{x}(t) + kx(t) = kz(t) + f_{ts}(x(t)), \tag{1}$$

where x is the position of the cantilever end, z is the position of the base, f_{ts} is the tip-to-sample force, and m, c, k are the effective mass, damping coefficient, and stiffness of the cantilever, respectively. To simplify the analysis, consider the time scaling $\tau = \omega_1 t$, where $\omega_1 = \sqrt{k/m}$ is the cantilever resonant frequency. Then (1) can be rewritten as

$$\ddot{x}(\tau) + \frac{1}{Q}\dot{x}(\tau) + x(\tau) = z(\tau) + \frac{1}{k} f_{ts}(x(\tau)), \tag{2}$$

where $Q = \sqrt{km}/c$ is the Q-factor.

Consider now that the base is excited with the bi-harmonic drive signal,

$$z(\tau) = a_1 \cos(\tau + \theta_1) + a_2 \cos(2\tau + \theta_2), \tag{3}$$

and make the following assumptions:

A1) The cantilever is in a stable, periodic solution and makes contact with the sample once per period.
A2) The cantilever is tapping in air or a vacuum, and thus $Q \gg 1$.
A3) The tip-to-sample force occurs quickly, over a small portion of the period (i.e., hard-contact tapping mode).

Following (A2), it is reasonable to model the tip-to-sample force as an impulse train,

$$f_{ts}(x(\tau)) \approx f_0 \sum_i \delta(\tau - 2\pi i + \theta_0), \tag{4}$$

where f_0 is the force magnitude and θ_0 is the phase of the tip-to-sample contact, which logically occurs at the lowest point of the probe trajectory, or,

$$\theta_0 = \underset{0 \le \theta < 2\pi}{\arg\min}\, x(\theta). \tag{5}$$

Using the Fourier description of the tip-to-sample force, (4),

$$f_{ts}(x) \approx \frac{1}{2\pi} + \frac{f_0}{\pi}\cos(\tau + \theta_0) + \frac{f_0}{\pi}\cos(2(\tau + \theta_0)) + \frac{f_0}{\pi}\cos(3(\tau + \theta_0)) + \cdots. \tag{6}$$

Noting that the large Q-factor (assumption A2) ensures that the first harmonic of the cantilever response will be much larger than the response to the higher harmonics, it is reasonable to neglect the higher harmonics, and thus (2) can be approximated as the linear system forced by two harmonics,

$$\ddot{x}(\tau) + \frac{1}{Q}\dot{x}(\tau) + x(\tau) = a_1 \cos(\tau + \theta_1) + a_2 \cos(2\tau + \theta_2) + \frac{1}{\pi k} f_0 \cos(\tau + \theta_0). \tag{7}$$

The solution to (7) takes the form

$$x(\tau) = x_1(\tau) + x_2(\tau) = A_1 \cos(\tau + \phi_1) + A_2 \cos(2\tau + \phi_2), \tag{8}$$

where $x_i(\tau)$ is the ith harmonic component of $x(\tau)$ and A_1, A_2, ϕ_1, ϕ_2 are parameters to be solved for. Substituting (8) into (7) yields

$$A_1 e^{j\phi_1} = Q e^{j\frac{\pi}{2}} \left(a_1 e^{j\theta_1} + \frac{f_0}{\pi k} e^{j\theta_0} \right), \tag{9}$$

$$A_2 e^{j\phi_2} = \frac{a_2 Q e^{j\theta_2}}{2e^{j\frac{\pi}{2}} - 3Q}, \tag{10}$$

and from (5),

$$\theta_0 = \underset{0 \le \theta < 2\pi}{\arg\min}\, A_1 \cos(\theta + \phi_1) + A_2 \cos(2\theta + \phi_2). \tag{11}$$

Thus, the trajectory shape can be obtained by simultaneously solving (8)–(11).

B. A broad-valley trajectory for improved measurement sensitivity

In Ref. 24 a so-called "broad-valley" trajectory was generated by selecting the first harmonic of the drive signal, a_1, to give the desired free-response amplitude, and then selecting,

$$\theta_1 = \tfrac{\pi}{2},\ \theta_2 = \pi \text{ and } 0 < a_2 < 0.75 Q a_1, \tag{12}$$

where larger values of a_2 give a wider valley to the trajectory. This particular trajectory shape demonstrated as much as 20% improvement in measurement sensitivity, though the mechanism behind the improvement was not well understood. The analysis in Sec. II A is used here to clarify that mechanism.

Figure 2 shows snapshots of single-harmonic and broad-valley bi-harmonic trajectories obtained from (8) to (11) at several points along the approach to the sample. The cantilever parameters $k = 15$ nN/nm, $Q = 300$ were chosen for the analysis. The first harmonic drive amplitude a_1 was chosen in such a way that the tip trajectory has free amplitude,

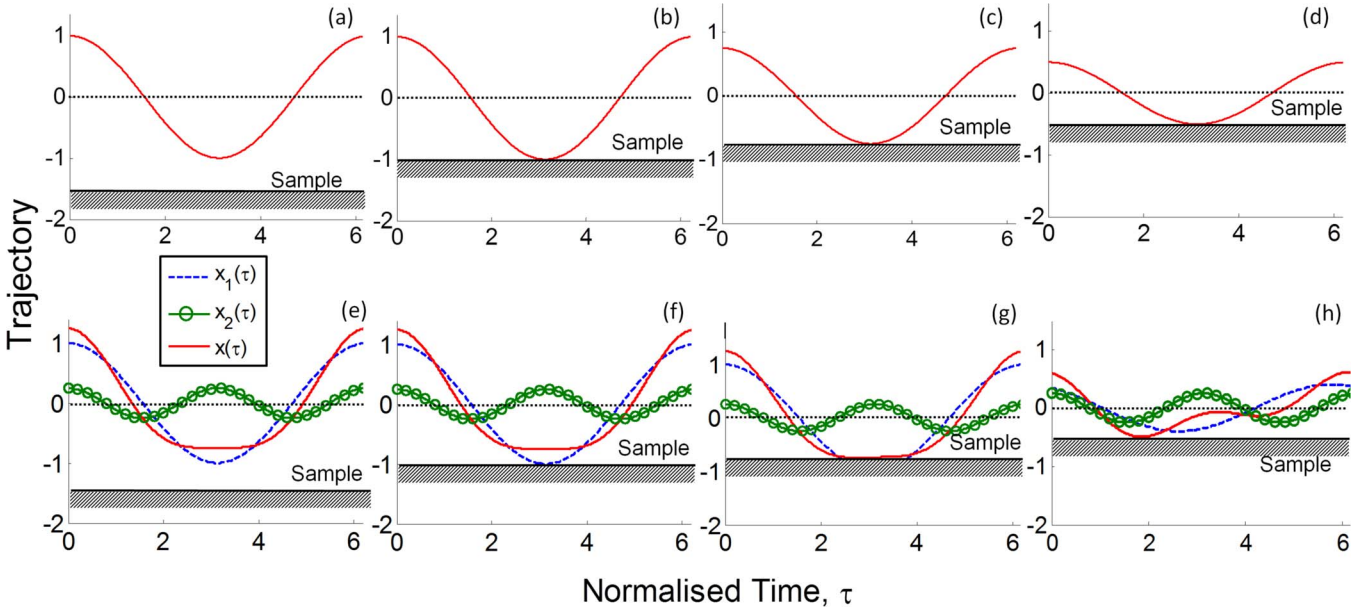

FIG. 2. Single-harmonic ($A_2 = 0$) and bi-harmonic ($A_2/A_{01} = 0.25$) trajectories at several different standoff distances from the sample obtained from the analytical model (8)-(11). Frames (a)–(d) are single-harmonic trajectories and (e)–(h) are bi-harmonic trajectories. Comparing (c),(d) to (g),(h), the bi-harmonic amplitude reduces more than the single-harmonic amplitude.

$A_{01} = 1$. The second harmonic drive amplitude was set to $a_2 = 0.75Qa_1$ which resulted in trajectory amplitude ratio $A_2/A_{01} = 0.25$. Several interesting features can be observed in Figure 2. First, the second harmonic remains invariant to the tip-to-sample distance, which can also be seen mathematically from (10), where A_2 and ϕ_2 are independent of f_0. Thus, only the first mode responds to contact with the sample. Second, while both single-harmonic and bi-harmonic trajectories have the same peak-to-peak free-response amplitude of 2, the lowest point on the broad-valley trajectory is closer to the nominal position of 0. Therefore, the sample is much closer to the nominal position before the bi-harmonic trajectory first makes contact. Contact for the single-harmonic response is made in frame (b) of Figure 2, but contact for the bi-harmonic is not made until frame (g). Consequently, while the amplitude of the single-harmonic response reduces gradually from frame (b) to frame (d), the bi-harmonic amplitude reduces dramatically from frame (g) to (h), thereby increasing the measurement sensitivity of the probe. Figure 3 shows the approach-retract curve predicted by (8)–(11) compared to the curve obtained from the numerical differential equation solutions of (1) (using the Lennard-Jones model given in Ref. 26 to model the tip-to-sample interaction force, f_{ts}).

III. BI-HARMONIC CANTILEVER DESIGN

A drawback of the bi-harmonic trajectory shaping design in (3) is that the piezo base-motion is approximately Q times larger at the 2nd harmonic than it is for the 1st harmonic. Because Q is typically very large, the piezo can saturate when trying to drive the 2nd harmonic. Here, a design is presented for a cantilever capable of generating bi-harmonic motion without large base motion at the 2nd harmonic. This is achieved by altering the geometry of the cantilever so that the 2nd eigenmode occurs at approximately twice the frequency of the 1st eigenmode.

A. Bi-harmonic trajectories for a bi-harmonic cantilever

Consider now the dynamics of the first two eigenmodes of a cantilever and assume that the resonant frequency of the 2nd eigenmode is exactly twice that of the 1st eigenmode.

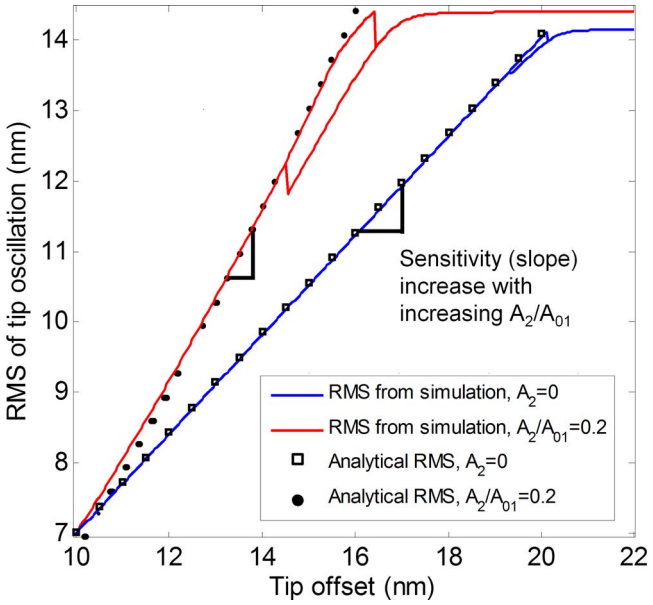

FIG. 3. RMS vs. tip sample offset (x_s) obtained through analytical framework and numerical simulation for single harmonic ($A_2 = 0$) and bi-harmonic ($A_2/A_{01} = 0.2$) trajectories. Numerical simulations show the well-known hysteretic loop that switches between hard-tapping and soft-tapping solutions. The analytical model matches the numerical simulation well throughout the hard-tapping portion of the approach-retract curve.

Then,

$$\begin{aligned}\ddot{x}_1(\tau)+\frac{1}{Q_1}\dot{x}_1(\tau)+x_1(\tau)&=z(\tau)+\frac{1}{k_1}f_{ts}(x)\\ \ddot{x}_2(\tau)+\frac{2}{Q_2}\dot{x}_2(\tau)+4x_2(\tau)&=z(\tau)+\frac{1}{k_2}f_{ts}(x)\\ x(\tau)&=x_1(\tau)+x_2(\tau),\end{aligned}\tag{13}$$

where x_1 and x_2 are the position components, Q_1 and Q_2 are the quality factor, and k_1 and k_2 are the stiffness of the first two eigenmodes, respectively. Consider, again, the Fourier description of the tip-to-sample force (6) and also the bi-harmonic base motion, (3), but now assume that the base-motion is small for each harmonic, that is, a_1 and a_2 are small. Then, (13) can be reasonably approximated as

$$\begin{aligned}&\ddot{x}_1(\tau)+\frac{1}{Q_1}\dot{x}_1(\tau)+x_1(\tau)\\ &\quad=a_1\cos(\tau+\theta_1)+\frac{1}{\pi k_1}f_0\cos(\tau+\theta_0)\\ &\ddot{x}_2(\tau)+\frac{2}{Q_2}\dot{x}_2(\tau)+4x_2(\tau)\\ &\quad=a_2\cos(2\tau+\theta_2)+\frac{1}{\pi k_2}f_0\cos(2\tau+\theta_0)\\ &x(\tau)=x_1(\tau)+x_2(\tau).\end{aligned}\tag{14}$$

Clearly, if the cantilever achieves a stable periodic solution, then the eigenmode trajectories take the form

$$\begin{aligned}x_1(\tau)&=A_1\cos(\tau+\phi_1)\\ x_2(\tau)&=A_2\cos(2\tau+\phi_2).\end{aligned}\tag{15}$$

However, the trajectory solutions are significantly more complicated than in the single-eigenmode analysis of Sec. II because both mode trajectories are dependent on f_0 and θ_0. However, it is possible to simplify the solution and dynamic behavior if the 2nd mode is significantly more stiff than the 1st mode, or $k_2 \gg k_1$. If $k_2 \gg k_1$, then it is possible to approximate (14) as

$$\begin{aligned}&\ddot{x}_1(\tau)+\frac{1}{Q_1}\dot{x}_1(\tau)+x_1(\tau)\\ &\quad=a_1\cos(\tau+\theta_1)+\frac{1}{\pi k_1}f_0\cos(\tau+\theta_0)\\ &\ddot{x}_2(\tau)+\frac{2}{Q_2}\dot{x}_2(\tau)+4x_2(\tau)=a_2\cos(2\tau+\theta_2)\\ &x(\tau)=x_1(\tau)+x_2(\tau),\end{aligned}\tag{16}$$

from which the stable periodic solution can be obtained as the solution to

$$A_1e^{j\phi_1}=Q_1e^{j\frac{\pi}{2}}\left(a_1e^{j\theta_1}+\frac{f_0}{\pi k_1}e^{j\theta_0}\right),\tag{17}$$

$$A_2e^{j\phi_2}=\tfrac{1}{4}a_2Q_2e^{j\theta_2},\tag{18}$$

$$\theta_0=\underset{0\le\theta<2\pi}{\arg\min}\,A_1\cos(\theta+\phi_1)+A_2\cos(2\theta+\phi_2).\tag{19}$$

Thus, the trajectory shaping for the bi-harmonic cantilever retains the essential features already developed for single-harmonic cantilevers. Namely, the first mode trajectory for the bi-harmonic cantilever, (17), has the same dependence as in the single-harmonic case, (9). Also, the second mode trajectory, (18), is independent of f_0, as in the single-harmonic case, (10). However, the significant difference is that a_2 is now similarly scaled to that of a_1 because of the Q_2 that appears in (18). Thus, the base excitation for the second harmonic is on the order of that used in the first harmonic. It remains to design a cantilever that meets the above assumptions. Specifically, the second mode frequency should be twice that of the first mode frequency and the second mode should be significantly stiffer than the first mode. The broad-valley bi-harmonic trajectory can be generated as long as $A_2/A_{01} < 0.25$. The drive parameters to obtain broad valley trajectory can be selected as

$$\theta_1,\theta_2=\frac{\pi}{2},\text{ and }0<a_2<{Q_1}/{Q_2a_1}.\tag{20}$$

B. A bi-harmonic cantilever

For nominal rectangular cantilevers the second resonant frequency is normally greater than twice its first resonant frequency ($F_2 \gg 2F_1$). Hence, in order to match the second resonant mode to the second harmonic, the cantilever has to be modified suitably. Resonant frequencies of rectangular cantilever can be varied by selectively removing material from high stress location corresponding to that mode.[27,28] This reduces the effective spring constant of that mode, which in turn reduces the frequency of the mode.

The proposed cantilever, whose dimensions are shown in Figure 4(a), has a similar design to Ref. 28. In the cantilever, an inner beam oscillates inside of the larger, original beam. The large inertia of the inner beam significantly lowers the 2nd bending mode frequency. The 2nd bending mode is also significantly stiffer than the 1st bending mode due to the higher order bending. A finite-element-analysis (FEA) of the beam design is performed and shown in Figure 4(b). The cantilever dimensions are selected to match that of a commercial silicon cantilever (TESP) manufactured by BRUKER (125 μm long, 40 μm wide, and 4 μm thick, 1st mode frequency of 350 kHz with stiffness of 42 nN/nm). Using an iterative process, the inner beam dimensions are adjusted in FEA software until the 2nd mode frequency was reduced to twice that of the 1st mode. The final dimensions of the inner beam which resulted in such a property are effective length (L_{eff}) of 84 μm and width of 16 μm. The 1st mode frequency was reduced from 350 kHz to 200 kHz, while the 2nd mode frequency was reduced from 2300 kHz to 400 kHz. The 1st mode stiffness was reduced from 42 nN/nm to 15 nN/nm and the 2nd mode stiffness after modification is 1355.2 nN/nm (significantly higher than the 1st mode stiffness). Following a similar procedure, it is possible to design a bi-harmonic cantilever from other standard single-beam AFM cantilever probes.

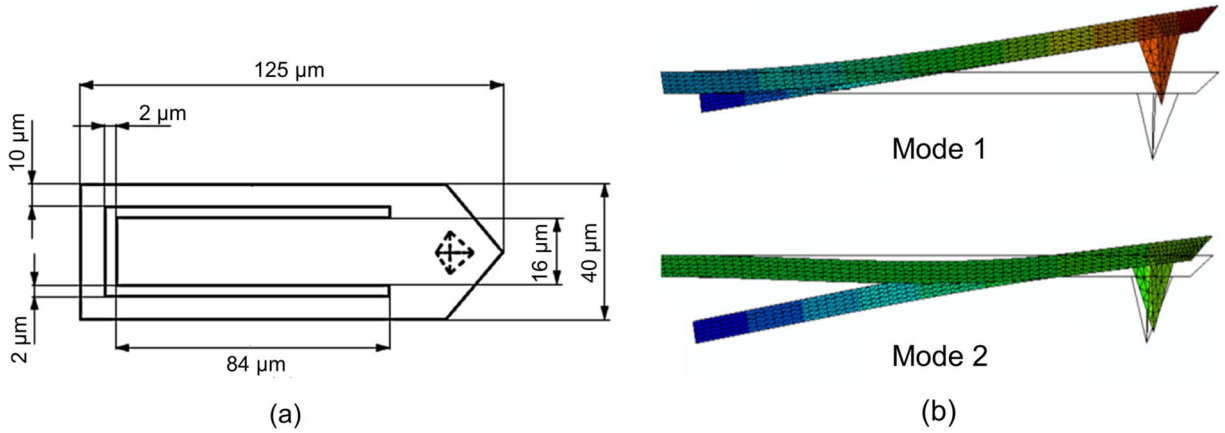

FIG. 4. (a) Bi-harmonic cantilever (b) first and second resonant mode shape of the cantilever with a fixed base and free end (tip). The resonant frequencies are 200 kHz and 400 kHz, respectively.

C. Bi-harmonic cantilever fabrication

The bi-harmonic cantilever is fabricated by milling out the inner cantilever on a BRUKER (TESP) commercial tapping-mode cantilever using an FEI Helios NanoLab 600 focused ion beam (FIB). An image of the fabricated beam is shown in Figure 5(a). Because of uncertainties in cantilever material properties and fabrication errors, the 2nd mode resonant frequency of the fabricated cantilever was typically not precisely twice that of the 1st mode resonant frequency. In these cases the resonant frequency was corrected by removing additional material, marked A and B in Figure 5(b). Material A was removed when the 2nd resonant mode frequency was too low, thereby shortening the inner beam and increasing its frequency. Material B was removed when the 2nd mode frequency is too high, thereby extending the length of the inner beam and reducing its frequency. The authors found that typically one or two iterations are sufficient to achieve the desired frequency ratio. The frequency response of a typical bi-harmonic cantilever is shown in Figure 6.

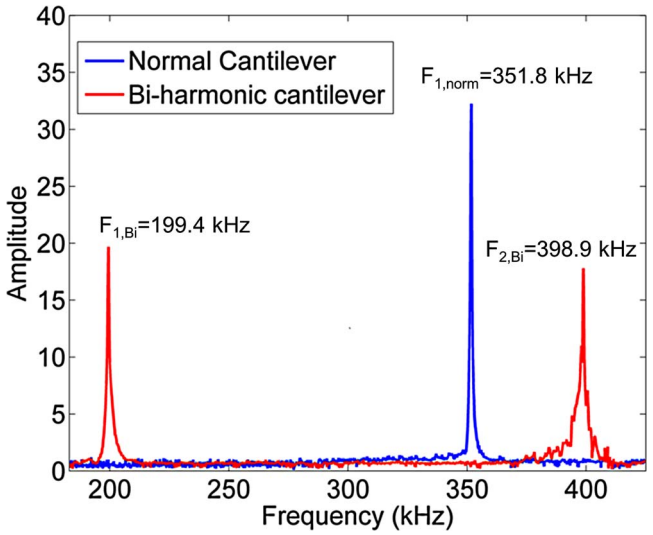

FIG. 6. Frequency response (input = base motion) of the normal (unmodified) cantilever and modified bi-harmonic cantilever shown in Figure 5.

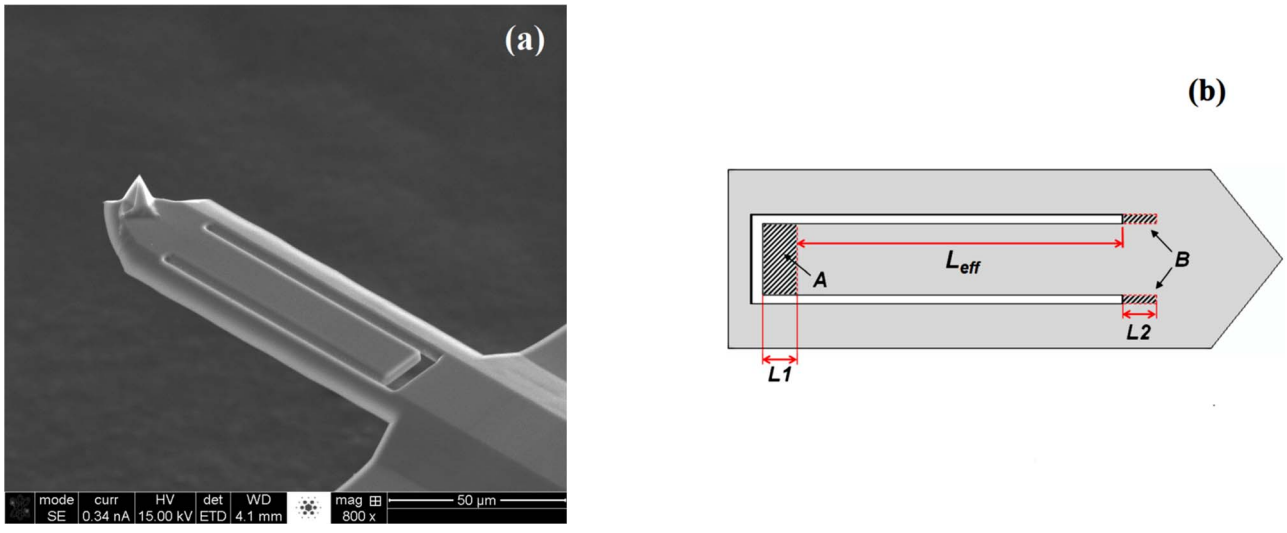

FIG. 5. (a) SEM image of bi-harmonic cantilever fabricated using Focused Ion Beam (FIB). (b) Top view of the cantilever showing dimensions that can be altered (L_1, L_2) to tune the 2nd mode of the cantilever.

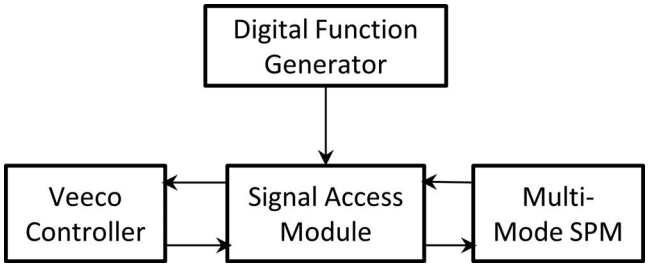

FIG. 7. Schematic of experimental AFM setup.

IV. EXPERIMENTAL RESULTS

Experiments were performed on a Veeco Multi-Mode scanning probe microscope with a cobalt test sample from Ted Pella, Inc. The default sinusoidal drive signal was replaced by bi-harmonic drive signal generated by a National Instruments digital function generator as in Figure 7. The bi-harmonic trajectory was shaped in free-response, before engaging the cantilever with the sample.

While, in theory, a broad-valley trajectory is generated with the parameters given in (20), in practice, variations in the cantilever and laser alignment require some tuning of the parameters. The tuning procedure, illustrated in Figure 8, is as follows:

(1) Adjust the first-harmonic drive amplitude, a_1, to obtain the desired free-response amplitude (A_{01}).
(2) Set θ_1, θ_2, as in (20) and increase a_2 until the 2nd harmonic is visible in the free-response trajectory
(3) Tune θ_2 to align the 2nd harmonic so that it widens the trajectory at the lowest point.
(4) Increase a_2 to widen the valley to the desired degree. If two minimum points appear, reduce a_2.

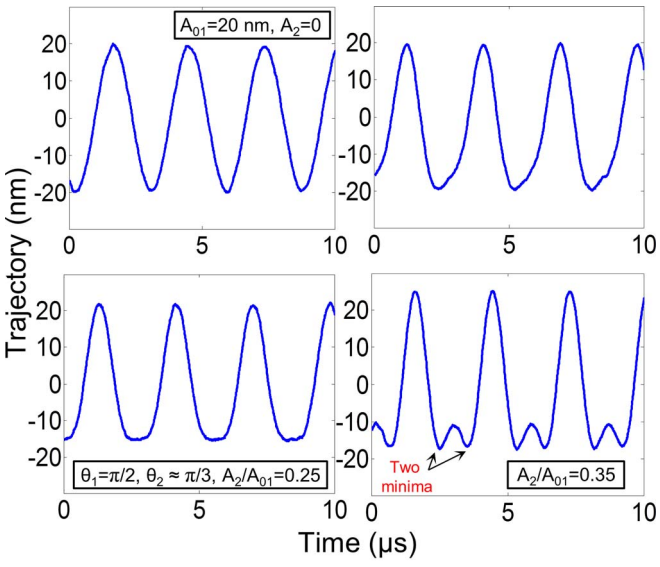

FIG. 8. Broad valley trajectory tuning procedure. (a) Step 1: 1st mode drive amplitude a_1 is chosen to give a desired free response amplitude, e.g., A_{01} = 20 nm (b) Step 2: Ideal θ_1, θ_2, and a_2 are selected as in (20). (c) Step 3: θ_2 is adjusted to obtain a broad valley trajectory. (d) Step 4: a_2 is increased. If a_2 is increased too far, two minimum points appear on the trajectory.

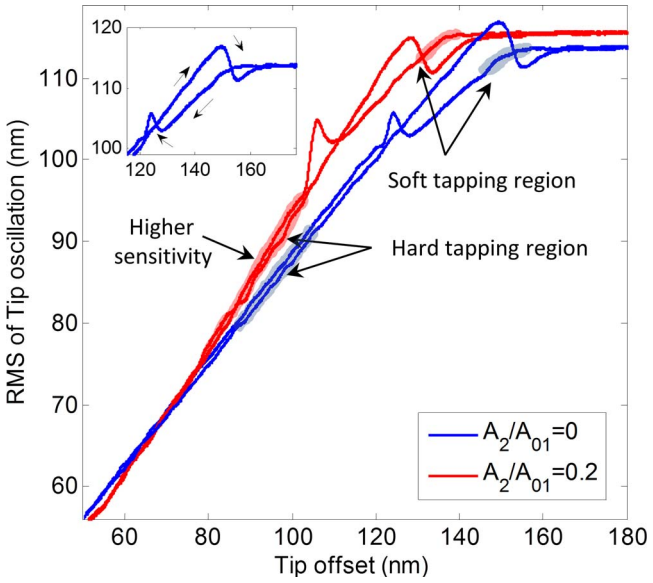

FIG. 9. Experimental RMS vs. tip sample offset curves of bi-harmonic cantilevers corresponding to single harmonic ($A_2/A_{01} = 0$) and bi-harmonic ($A_2/A_{01} = 0.2$) trajectory. Inset shows the approach and retract direction. The bi-harmonic curve has a higher slope, and thus a higher sensitivity.

It may help to use a FFT analysis of the measured trajectory to help in the tuning process. For a broad-valley trajectory the desired relationships between the 1st and 2nd harmonic parameters are

$$\phi_2 = 2\phi_1 \text{ and } 0 < A_2/A_{01} < 0.25. \quad (21)$$

A. Approach-retract curve validation

An experiment was setup such that the sample approaches and retracts from the tip at a constant rate of 2000 nm/s, and the RMS (volts) value of the reflected laser signal from the photo detector was recorded. Figure 9 shows the experimental approach-retract curves of the bi-harmonic cantilever with free RMS amplitude of 115 nm and amplitude ratio, $A_2/A_{01} = 0$ and 0.2. As the tip offset is reduced, the amplitude reduces and the probe enters into a bi-stable region where two stable solution states exist. These are referred to as attractive and repulsive solutions and are characterized by a hysteric loop. As the tip offset is further reduced, the repulsive solution becomes predominant and a linear relationship between the cantilever amplitude and tip offset can be observed. The experimental sensitivity was calculated by measuring the slope of this linear region ($60 \leq x_s \leq 100$ nm) of the experimental data. The sensitivity improvement compared to single harmonic tapping is approximately 33%.

In another experiment, the frequency response of the bi-harmonic cantilever was measured by injecting sine waves into the Z piezo control channel and measuring the frequency response of the cantilever RMS. The response of the bi-harmonic cantilever is shown in Figure 10 for both the single harmonic trajectory and bi-harmonic trajectory. As can be seen, the bi-harmonic trajectory results in an increased magnitude, or measurement sensitivity, across the entire bandwidth

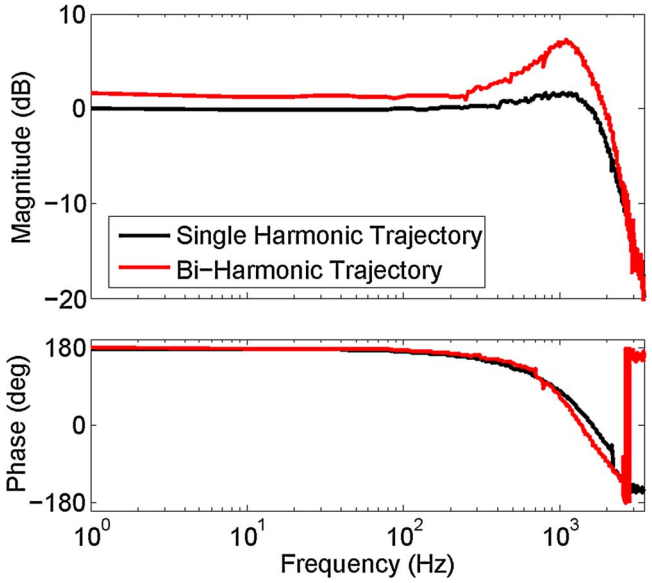

FIG. 10. Experimental frequency response of RMS vs. sinusoidally varying Z piezo position for bi-harmonic cantilevers corresponding to single harmonic ($A_2/A_{01} = 0$) and bi-harmonic ($A_2/A_{01} = 0.2$) trajectory. The bi-harmonic trajectory has a higher sensitivity (shown by a larger magnitude) across the entire range of frequencies before the high frequency rolloff.

of the cantilever. At low frequencies the increased sensitivity is 1.66 dB, or 21% and at higher frequencies the sensitivity is 5.42 dB, or 87% larger.

Secs. IV B–IV D, we examine the quality of images obtained using the bi-harmonic broad-valley trajectory and compare with those obtained from a standard single-harmonic trajectory. The increased measurement sensitivity of the bi-harmonic method produces a larger signal for similarly sized changes in the sample height, resulting in a more aggressive correction by the feedback controller, and thus reducing image error. The broad-frequency improvement reduces imaging errors across the entire frequency range of the cantilever bandwidth. Several imaging scenarios are considered.

1. Case I: Low-speed imaging in the hard-tapping region

In low-speed imaging, the majority of the image content is located in low frequencies, where errors are small and below the noise floor. The noise floor will mask any difference between single-harmonic and bi-harmonic methods in the low frequency region. However, a small portion of the image content may appear at higher frequencies, above the noise floor. In this case, the higher sensitivity of the bi-harmonic method will track these frequencies better, but may not be visually apparent if the image is dominantly in the low-frequency region.

2. Case II: Higher-speed imaging in the hard-tapping region

By scanning at higher speeds, a larger portion of the image content will move into the higher-frequency region where the tracking errors dominate measurement noise. Both single-harmonic and bi-harmonic methods will appear degraded and blurry compared to their lower speed counterparts. However, the higher sensitivity of the bi-harmonic method will result in lower degradation.

3. Case III: Low-speed imaging in the soft-tapping region

The soft-tapping region is not typically used for imaging because of the hysteretic loop (Figure 9) that coincides with this region. However, when imaging fragile samples, the soft-tapping region is sometimes necessary. The measurement sensitivity in the soft-tapping region is much less than in the hard-tapping region (as evidenced by the lower slopes of the approach-retract curves), resulting in large image errors above the noise level, even at low speeds. While the quality of the images will be lower in soft-tapping than in hard-tapping for both single-harmonic and bi-harmonic methods, the higher sensitivity of the bi-harmonic trajectory will provide a clearer image.

B. Case I: Low-speed imaging in hard-tapping region

A bi-harmonic cantilever was used for imaging a cobalt sample with free RMS amplitude of 115 nm and set point amplitude of about 85 nm. The sample was scanned at 1 Hz over an area of 1×1 μm. The proportional and integral gains for the controller were set to 0.85 and 0.7, respectively. From Figure 9 it is clear that 85 nm RMS amplitude set point is in the hard tapping region, below the hysteretic loop region, which is the typical region for imaging. As discussed above, the difference between single-harmonic and bi-harmonic methods in low-speed imaging in the hard-tapping region will not be easily perceptible in the image because most of the tracking error is below the noise floor. This can be seen in Figure 11(a) where the tapping trajectory was changed from single to bi-harmonic ($A_2/A_{01} = 0.2$) half way through the scan while the controller gains were kept constant. However, it is possible to detect that the tracking performance (and thus image quality) is better at higher frequencies using the bi-harmonic method. A Fourier image analysis of the single-harmonic and bi-harmonic images is performed and a thresholding of the Fourier image spectra are shown in Figure 11(b). The Fourier image analysis gives the spatial frequency of the image in its horizontal and vertical components.

One measure of the sharpness of an image is the radius of the cluster of points in the middle of the Fourier image spectra.[29] As seen in Figure 11(b), the larger radius of the cluster on the bi-harmonic image spectra indicates that the bi-harmonic image is sharper than the single-harmonic image. The reader may be able to observe the improved sharpness of the image in Figure 11(a) with a high-resolution copy of this paper.

C. Case II: Higher-speed imaging in hard-tapping region

As the scan speed is increased, spatial frequencies map to higher temporal frequencies. In the higher-frequency

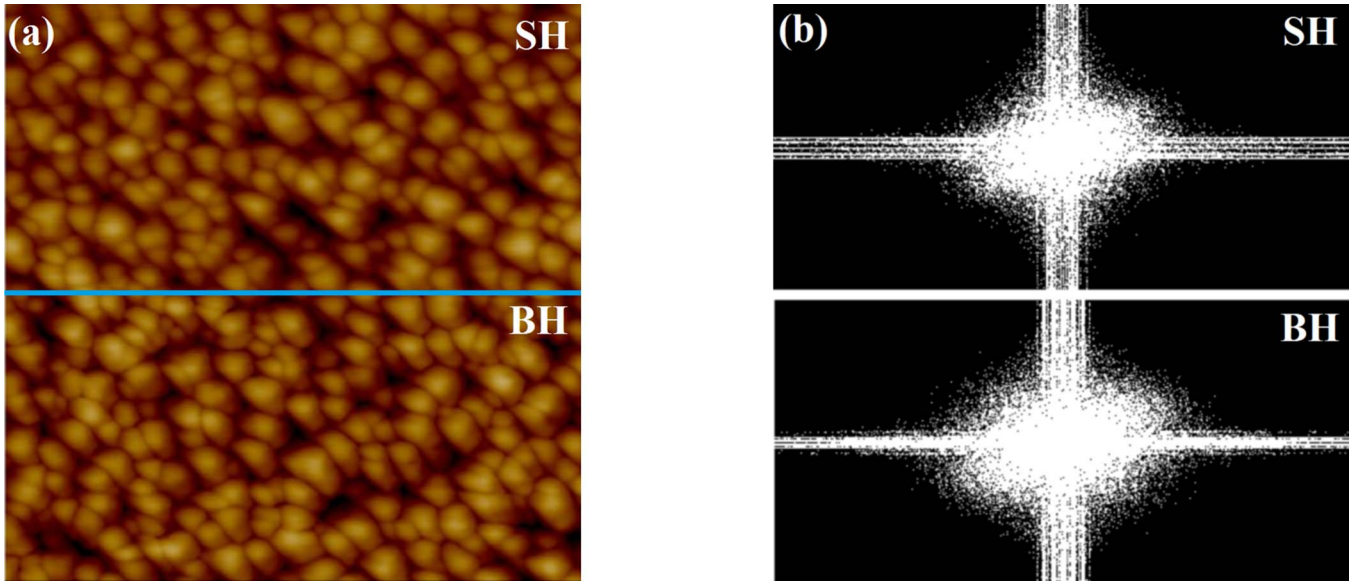

FIG. 11. (a) Surface image (1×1 μm) of cobalt sample scanned at 1 Hz. The tapping trajectory was changed mid-way through the scan from single harmonic ($A_2/A_{01} = 0$) to bi-harmonic ($A_2/A_{01} = 0.2$). (b) Fourier image transform of single and bi-harmonic sections of (a). Note: SH indicates single harmonic tapping and BH indicates bi-harmonic tapping.

region the tracking error will dominate noise and image error will increase. Although image quality will reduce for both the single-harmonic and bi-harmonic images when compared to the lower scan speed (Case I), the bi-harmonic image will be less affected because of its higher sensitivity.

The cobalt sample was again imaged with the same parameters as in Sec. IV B, except that the scan speed was increased to 5 Hz. Figure 12(a) shows the acquired image with the top half using single-harmonic and then switching to bi-harmonic ($A_2/A_{01} = 0.2$) half way through the scan. The better quality of the bi-harmonic image compared to the single-harmonic is visually recognizable, confirming the benefit of higher loop sensitivity function bandwidth in higher-speed imaging.

D. Case III: Low-speed imaging in soft tapping region

In soft tapping the measurement sensitivity is much lower than in hard-tapping, and thus even at low speeds the image accuracy can be poor. Figure 13 shows cobalt surface image obtained by operating in the soft tapping region with the tapping trajectory switched from single to broad valley midway through. The image was obtained by scanning an area of

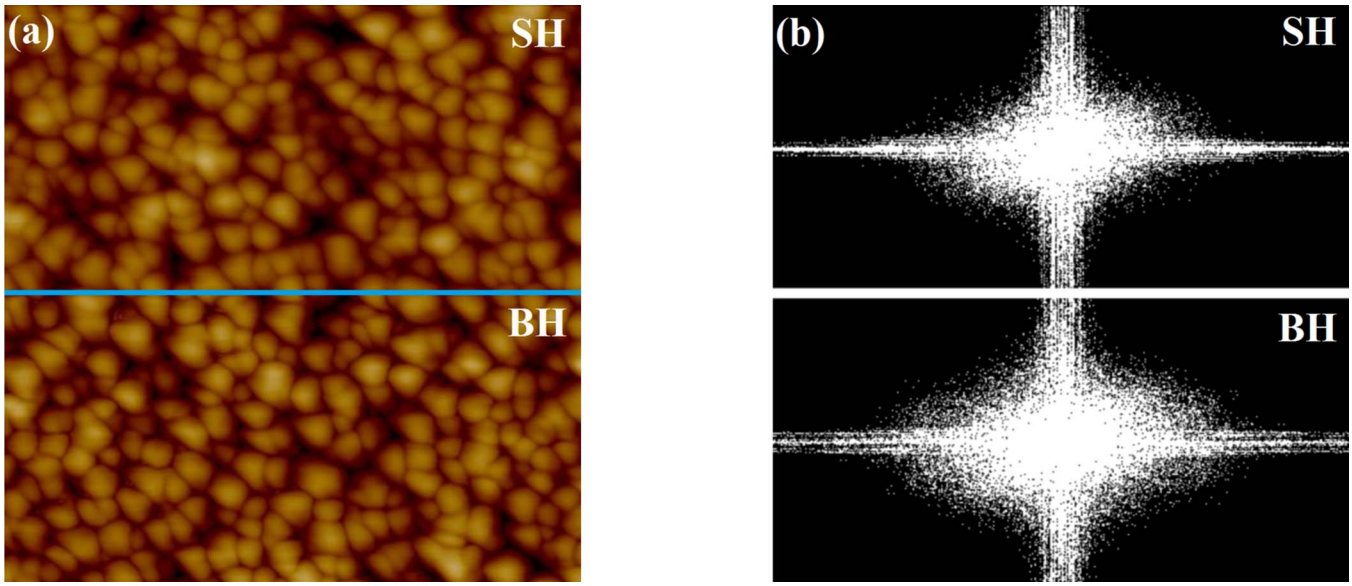

FIG. 12. (a) Surface image (1×1 μm) of cobalt sample scanned at 5 Hz. The tapping trajectory was changed mid-way through the scan from single harmonic ($A_2/A_{01} = 0$) to bi-harmonic ($A_2/A_{01} = 0.2$). (b) Fourier image transform of single and bi-harmonic sections of (a). Note: SH indicates single harmonic tapping and BH indicates bi-harmonic tapping.

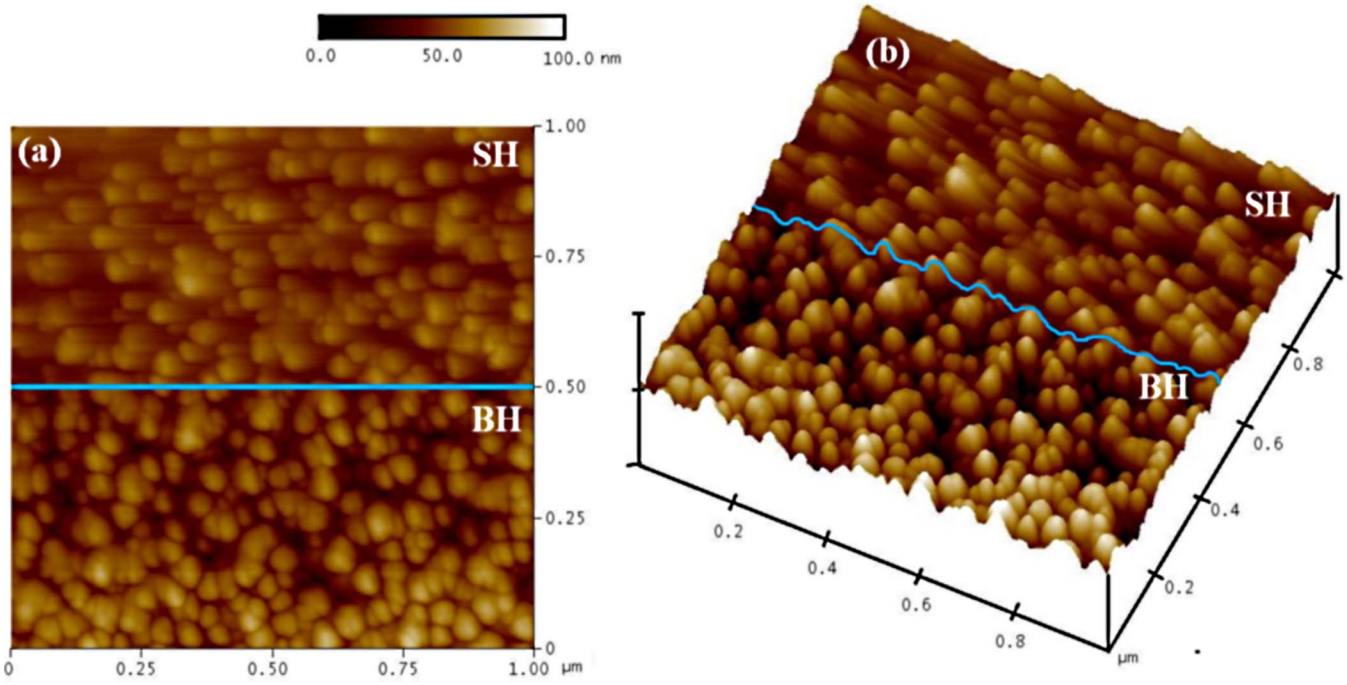

FIG. 13. Cobalt sample (1×1 μm) scan with the tapping trajectory changed to bi-harmonic ($A_2/A_{01} = 0.2$) mid-way through the scan. (a) Two-dimensional surface height image. (b) Three-dimensional representation of (a). Note: SH indicates single harmonic tapping and BH indicates bi-harmonic tapping.

1×1 μm at 1 Hz scan speed with the same controller gains and bi-harmonic amplitude ratio ($A_2/A_{01} = 0.2$) as in Sec. IV B. The free RMS amplitude of the cantilever was set to 115 nm with RMS set point amplitude fixed around 110 nm. In single harmonic operation, low sensitivity resulted in poor surface tracking, generating a blurry image. However, when the trajectory was switched to bi-harmonic, the higher sensitivity resulted in a stronger signal for the feedback controller, and thereby improved the surface tracking. The result is a sharp and detailed image.

V. CONCLUSIONS

In summary, we have presented a novel idea of improving the mechanical sensitivity of TM-AFM probe through trajectory shaping. In this method, the conventional sinusoidal tapping trajectory is altered by driving the cantilever with drive signal composed of a 2nd harmonic at twice the frequency of the primary harmonic. Mathematical analysis shows that by maintaining appropriate amplitude and phase at the first and second harmonic frequencies the tapping trajectory can be reshaped into a broad valley trajectory, whose inherent characteristic (offset) results in improved measurement sensitivity. The theory behind this effect has also been presented. Though rectangular AFM cantilevers respond to bi-harmonic drive signal, large drive force is required at the second harmonic to achieve decent trajectory shaping. Given the constraints on electronic hardware such a force may not be realizable. In order to overcome this issue we have developed a cantilever design whose 2nd resonant frequency is twice its 1st resonant frequency. This property makes the new cantilever readily respond to bi-harmonic drive signal. Such a cantilever was fabricated from a standard commercial cantilever using a FIB.

Experiments show that bi-harmonic trajectories improve measurement sensitivity by 30% compared to sinusoidal tapping. While useful in standard imaging applications to obtain the most accurate measurements, the approach appears to be especially useful in non-ideal imaging conditions like high speed scanning and in weak force fields where the sensitivity of sinusoidal trajectory is poor. In these conditions, broad valley tapping renders significantly sharper and more accurate images.

ACKNOWLEDGMENTS

This work was supported by the National Science Foundation (NSF), CMMI-1229701, and the Missouri University of Science and Technology Materials Research Center

[1]G. Binnig, C. F. Quate, and C. Gerber, Phys. Rev. Lett. **56**, 930 (1986).
[2]A. D. L. Humphris, M. J. Miles, and J. K. Hobbs, Appl. Phys. Lett. **86**, 034106 (2005).
[3]T. Ando, Nanotechnology **23**, 062001 (2012).
[4]M. Gauthier, S. Sasaki, and M. Tsukada, Phys. Rev. B **64**, 085409 (2001).
[5]G. Couturier, J. P. Aime, J. Salardenne, and R. Boisgard, J. Phys. D **34**, 1266 (2001).
[6]F. J. Giessibl, Appl. Phys. Lett. **76**, 1470 (2000).
[7]S. Alexander, L. Hellemans, O. Marti, J. Schneir, and V. Elings, J. Appl. Phys. **65**, 164 (1989).
[8]N. P. D'Costa and J. H. Hoh, Rev. Sci. Instrum. **66**, 5096 (1995).
[9]D. R. Sahoo, A. Sebastian, and M. V. Salapaka, Int. J. Robust Nonlinear Control **15**, 805 (2005).
[10]G. Schitter, P. Menold, H. F. Knapp, F. Allgöwer, and A. Stemmer, Rev. Sci. Instrum. **72**, 3320 (2001).
[11]T. E. Schäffer, Nanotechnology **16**, 664 (2005).
[12]M. Stark, R. W. Stark, W. M. Heckl, and R. Guckenberger, Appl. Phys. Lett. **77**, 3293 (2000).
[13]J. Tamayo, Appl. Phys. Lett. **75**, 3569 (1999).

[14]R. W. Stark and W. M. Heckl, Surf. Sci. **457**, 219 (2000).
[15]R. Hillenbrand, M. Stark, and R. Guckenberger, Appl. Phys. Lett. **76**, 3478 (2000).
[16]R. W. Stark and W. M. Heckl, Rev. Sci. Instrum. **74**, 5111 (2003).
[17]R. W. Stark, T. Drobek, and W. M. Heckl, Appl. Phys. Lett. **74**, 3296 (1999).
[18]S. J. T. Van Noort, O. H. Willemsen, K. O. Van der Werf, B. G. de Grooth, and J. Greve, Langmuir **15**, 7101 (1999).
[19]R. W. Stark, N. Naujoks, and A. Stemmer, Nanotechnology **18**, 065502 (2007).
[20]T. R. Rodríguez and R. García, Appl. Phys. Lett. **84**, 449 (2004).
[21]N. F. Martinez, S. Patil, J. R. Lozano, and R. Garcia, Appl. Phys. Lett. **89**, 153115 (2006).
[22]J. R. Lozano and R. Garcia, Phys. Rev. Lett. **100**, 076102 (2008).
[23]O. Sahin, C. F. Quate, O. Solgaard, and A. Atalar, Phys. Rev. B **69**, 165416 (2004).
[24]M. Loganathan, S. R. Kodandarama, and D. A. Bristow, Rev. Sci. Instrum. **82**, 103704 (2011).
[25]A. Sebastian, A. Gannapalli, and M. V. Salapaka, IEEE Trans. Control Syst. Technol. **15**, 952 (2007).
[26]J. Israelachvili, *Intermolecular and Surface Forces* (Academic Press, Boston, 1985).
[27]O. Sahin, G. Yaralioglu, R. Grow, S. F. Zappe, A. Atalar, C. Quate, and O. Solgaard, Sens. Actuators A **114**, 183 (2004).
[28]J. R. Felts and W. P. King, J. Micromech. Microeng. **19**, 115008 (2009).
[29]M. T. Postek and A. E. Vladár, Scanning **20**, 1 (1998).